Magnetic Resonance Imaging 31 (2013) 1372–1383

Contents lists available at ScienceDirect

Magnetic Resonance Imaging

journal homepage: www.mrijournal.com

Error bounds in diffusion tensor estimation using multiple-coil acquisition systems ☆

Leandro Beltrachini *, Nicolás von Ellenrieder, Carlos Horacio Muravchik

LEICI, Facultad de Ingeniería, Universidad Nacional de La Plata, Calle 1 y 47, B1900TAG, La Plata, Buenos Aires, Argentina

ARTICLE INFO

Article history:
Received 2 November 2012
Revised 23 April 2013
Accepted 26 April 2013

Keywords:
Cramér–Rao bound
Noncentral chi distribution
Measurement noise

ABSTRACT

We extend the diffusion tensor (DT) signal model for multiple-coil acquisition systems. Considering the sum-of-squares reconstruction method, we compute the Cramér–Rao bound (CRB) assuming the widely accepted noncentral chi distribution. Within this framework, we assess the effect of noise in DT estimation and other measures derived from it, as a function of the number of acquisition coils, as well as other system parameters. We show the applications of CRB in many actual problems related to DT estimation: we compare different gradient field setup schemes proposed in the literature and show how the CRB can be used to choose a convenient one; we show that for fiber-type anisotropy tensors the ellipsoidal area ratio (EAR) can be estimated with less error than other scalar factors such as the fractional anisotropy (FA) or the relative anisotropy (RA), and that for this type of anisotropy tensors, increasing the number of coils is equivalent to increasing the signal-to-noise ratio, i.e., the information of the different coils can be regarded as independent. Also, we present results showing the CRB of several parameters for actual DT-MRI data. We conclude that the CRB is a valuable tool to optimal experiment design in DT-related studies.

1. Introduction

Diffusion-weighted imaging is a magnetic resonance imaging (MRI)-based technique which can be used to characterize the structure of biological tissues in vivo, such as brain white matter [1]. It consists of measuring the diffusivity of water molecules in many directions to analyze the orientation-dependent water mobility, related to the structure of the internal medium. The diffusion phenomena in the tissues is not free, since the water molecules diffuse faster in directions aligned with the organs' inner structure and slower in the direction perpendicular to the enclosing membrane. Then, the resulting information is valuable to characterize the anatomical structure of soft tissues noninvasively.

If we assume a Gaussian probability density function for the diffusion phenomena, this mobility will be mathematically described by the diffusion tensor (DT) [1]. The DT is a simple model that represents the mobility of water molecules in any volume of interest by means of an ellipsoid whose semi-axis lengths are proportional to the diffusivity in the semi-axis directions. Mathematically, the DT is a 3×3 matrix whose eigenvectors and eigenvalues define the direction and length of each semi-axis. Given a number of diffusion measurements, the DT is estimated with some criteria [1,2]. Then, the main goal in DT-MRI studies lies in the estimation of the DT on each voxel where the MR pulse echo is measured, obtaining a three-dimensional DT map.

Many applications arise from the estimated DT map. One of them is the quantification of the anisotropy of the white matter by computing scalar and vector indices widely used in clinical practice, such as the fractional anisotropy (FA) or the relative anisotropy (RA). Their computation helps, for example, to make clinical diagnosis, as in various central nervous systems disorders. Also, the DT map is used to make in vivo fiber tractography studies [3], which is helpful for assessing the degree of invasiveness of neoplasms to specific functional tracts and for elucidating functional and anatomical connectivity, among other uses [3,4].

As the DT-MRI measurements are corrupted by noise, every function of the DT estimator will have some error. Even if the variance of the error can be reduced by appropriately adjusting the acquisition system, there exist theoretical limits that bound the estimation errors in any practical situation. These limits are of interest to the scientific community since they allow to define the scope of the technique and to optimize the system configuration in

☆ This work was supported by the Universidad Nacional de La Plata (UNLP) under grant no. 11-I-166, by the Consejo Nacional de Investigaciones Científicas y Técnicas (CONICET), by the Comisión de Investigaciones Científicas de la Provincia de Buenos Aires (CICpBA) and by the Agencia Nacional de Promoción Científica y Tecnológica (ANPCyT) under grant no. PICT 2011-0909.

* Corresponding author. Tel.: +54 0221 4259306.
E-mail address: lbeltra@gmail.com (L. Beltrachini).

0730-725X/$ – see front matter © 2013 Elsevier Inc. All rights reserved.
http://dx.doi.org/10.1016/j.mri.2013.04.009

order to reach them. Several works have considered the influence of noise in the estimation of scalar indices by means of error propagation techniques (e.g., Refs. [5,6]). However, this approach does not handle appropriately the noise distribution, leading to possible inaccuracies in the results. We propose using the Cramér–Rao bound (CRB) to deal with this problem.

The CRB gives the minimum variance that can be achieved by any unbiased estimator of the DT and the functions of it, independently of the estimation algorithm. This can be used to optimize the bounds in DT estimation as a function of tunable parameters. It has been used to investigate the scope of the technique in some experiments, such as in the study of the feasibility of measuring direct features of brain-tissue microstructure (as axon density and radius in white matter) [7] or in the analysis of diffusion properties in crossing fiber bundles [8]. These articles present the CRB as a valuable tool when a single acquisition coil montage is used, leading to expressions that may be inaccurate in multiple-coil acquisition montages. These latter systems have been proved to enhance the performance of MR-based studies [9] and were discussed only in a few papers within the DT-MRI community [10–13].

In this work, we propose a model for diffusion signals acquired with multiple-coil MR systems, adapted from parallel MR (pMR) background [9,14]. Then, we generalize the CRB for this case, to study the theoretical limits in the DT estimation and in the functions of it. Indeed, once the mathematical framework is presented, we apply it to get results related to some recent studies. First, we analyze the influence of the gradient field scheme adopted for the acquisition in the estimation of the DT by computing the minimum achievable variance. This is very important since there exist many gradient schemes presented in the literature, each of them optimal in some sense [5,15–17]. In this context, the CRB is presented as a statistical tool for comparing the proposed schemes considering the DT estimation bounds, providing a direct link between the gradient scheme and the DT estimation results.

Then, we analyze the minimum variance achievable in the estimation of different scalar functions of the DT elements. These functions could be the eigenvalues or the functions of them, such as the RA, the FA or the ellipsoidal area ratio (EAR) [18]. In this context, the CRB is used as a benchmark to compare the performance of the scalar functions estimation. This is relevant to applications, such as tractography, where the FA is generally used as a threshold in fiber reconstruction [3].

The analysis of the minimum standard deviation in the estimation of the DT major eigenvector is also of great interest [19], since in tractography applications the direction of the fiber is usually selected parallel to the major eigenvector [3]. Since this eigenvector is a function of the DT elements, it has an associated covariance, which must be properly studied when analyzing the confidence regions of the reconstructed tracts. Thus, we find the CRB associated with the major eigenvector estimation and evaluate the minimum angular deviation of any unbiased estimator with respect to its true value. We examine the variation of such error bound as a function of the MR system parameters and show how to reach optimal estimation conditions.

We also explore the relevance of the multiple-coil model and evaluate the differences with the single-coil montage [7]. This allows us to validate the assumption of statistical independence among coils in order to simplify the signal model for multiple-coil montages.

All these studies are made by varying some parameters of interest, such as the signal-to-noise ratio (SNR), the diffusion weighting b value, the number of acquisition coils, and the tensor shape (i.e., disc-, oblate- or spherical type). Results are shown using synthetic as well as real data.

2. Materials and methods

2.1. Signal and noise models

The main problems in DT-MRI applications are the limited spatial resolution and SNR achievable with a single-coil acquisition system. Therefore, multiple-coil acquisition systems (originally proposed in Ref. [14]) were adapted from the MRI framework to ensure better spatial resolution and higher SNR (e.g., Ref. [20]). In this section, we present the adopted signal model. First, we review the pMR statistical signal model. Then, we present a parallel DT-MRI statistical model that incorporates the multiple-coil acquisition setup.

2.1.1. MR signal model

MR data are usually modeled as a complex Gaussian process, where the real and imaginary parts of the original signal are corrupted with uncorrelated Gaussian noise with zero mean and equal variance σ^2. Some authors studied the statistical properties of noise for a single-coil acquisition system, concluding that it is reasonable to consider the magnitude of the received signal as Rice distributed or as Rayleigh distributed in case of no-signal state [21,22]. These models are important for many applications, such as estimating the SNR or the contrast-to-noise ratio (CNR), among others [21].

However, single-coil acquisition systems have some limiting properties, such as the acquisition speed or the maximum SNR achievable. To improve these aspects, multiple-coil acquisition systems were proposed [9,14]. These systems have the advantage of allowing to choose the method used to fuse the information measured by each RF acquisition coil. If we want to improve the SNR and the coil montage is completely known, the spatial matched filter approach is adequate [23]. On the other hand, if the coil montage is completely characterized and we want to speed up the acquisition time, some methods can be used, such as the generalized auto-calibrating partially parallel acquisition (GRAPPA) algorithm [24] in the frequency domain or the sensitivity-encoded MRI (SENSE) [25] in the image domain. Nevertheless, even if these methods are most adequate, it is infrequent in clinical practice to know the complete characterization of the coil system used, and it is unusual to have access to the technical settings of the MR machine. In these cases, the sum-of-squares (SoS) technique is the recommended method [9,14,26] and the one adopted for the analysis presented in this work.

Let S_l be the complex signal measured by the lth coil and A_l be the complex signal without noise in the same coil. Then, if we assume no magnetic coupling among the RF coils, the measured signal will be

$$S_l = \rho_l(p)A_l + \xi,$$

where $\rho_l(p)$ is the sensitivity of the lth coil in the space point p and ξ is a zero-mean complex Gaussian random variable with variance σ^2. Then, the SoS output of an L-coil system will be $S_T = \sqrt{\sum_{l=1}^{L} |S_l|^2}$ [21]. Under these assumptions, it can be shown that the SoS method will return, in the presence of signal, a noncentral chi distribution, with probability density function [22]

$$f(S_T; A_T, \sigma, L) = \frac{A_T^{1-L}}{\sigma^2} S_T^L exp\left(-\frac{S_T^2 + A_T^2}{2\sigma^2}\right) I_{L-1}\left(\frac{A_T S_T}{\sigma^2}\right), \quad (1)$$

where $A_T = (\sum_{l=1}^{L} |\rho_l(p)A_l|^2)^{1/2}$ and $I_\alpha(\cdot)$ is the αth-order modified Bessel function of the first kind. Note that (1) reduces to a Rician distributed signal if a single-coil system is used (i.e., $L = 1$).

A general SoS framework must consider the differences among the variance on each coil, leading to a generalized noncentral chi distribution [22]. However, in practical situations the noise variance is homogeneous enough across pixels and coils [23], and then data

are usually considered to follow a noncentral chi distribution when reconstructed with SoS or GRAPPA [23].

2.1.2. Parallel DT-MRI signal model

As stated before, DT-MRI is a technique that allows to measure the anisotropy of the media and characterize the internal structure of brain tissues in vivo and noninvasively. This is done by applying a magnetic field gradient sequence in a number of directions, after which the echo attenuation in each voxel is measured. Then, the measurement depends on the applied sequence and the gradient field direction and strength. Some of these parameters are summarized in the diffusion weighting parameter b (called b value), which selects the diffusivity scale of measurements and depends on the gradient strength and diffusion time [1]. With the use of conventional pulsed-gradient spin-echo (PGSE) sequence, the diffusion time is $\Delta-\delta/3$, where Δ is the time between both gradients and δ the diffusion weighting gradient duration [1]. Then, the b value is defined as $b=\gamma^2\delta^2(\Delta-\frac{\delta}{3})g_a^2$ [27], where γ is the gyromagnetic constant and g_a is the magnitude of the applied gradient field, usually between 1000 s/mm^2 and 3000 s/mm^2.

If we assume a Gaussian distribution for the diffusion phenomenon, the signal intensity measured in the lth coil when the nth gradient field is applied will be [26]

$$S_{ln}=\rho_l(p)A_n+\xi,$$

where $A_n=S_0 exp(-g_n^{\mathrm{T}}\theta)$, S_0 is the signal measured when no gradient field is applied, g_n is a six-element vector related to the gradient field direction and to the b value, and $\theta=[\theta_1,\cdots,\theta_6]^{\mathrm{T}}$ is the six-element vector rearrangement of the DT elements,

$$D=\begin{pmatrix}\theta_1 & \theta_4 & \theta_5\\ \theta_4 & \theta_2 & \theta_6\\ \theta_5 & \theta_6 & \theta_3\end{pmatrix}.$$

(see Appendix A for g_n definition and Ref. [27] for model details). Note that, since we are only interested in the signal intensity, its phase is not taken into account and the signal intensity without noise will only vary among coils depending on their sensitivity pattern.

If we consider independence among coils (i.e., totally decoupled coils) and the same standard deviation in each measurement, the SoS method can be applied and the measurement will be distributed according to Eq. (1). Using previous definitions, it is easily found that, when the nth gradient field is applied, the SoS signal will be distributed according to the probability density function $f(S_{Tn};A_{Tn},\sigma,L)$, where $S_{Tn}=(\sum_{l=1}^{L}|S_{ln}|^2)^{1/2}$ is the SoS signal, $A_{Tn}=C_L(p)S_0 exp(-g_n^{\mathrm{T}}\theta)$ is the DT signal model considering the multiple-coil montage, and $C_L(p)=(\sum_{l=1}^{L}\rho_l^2(p))^{1/2}$ is the sensitivity factor in p.

2.2. Performance bounds

The main goal of this work was to study the influence of measurement errors in the DT estimation and in the functions of it. This is done with the help of the Cramér–Rao inequality, which gives a lower bound on the variance of any unbiased estimator, regardless of the estimation algorithm used [28]. Let $z(\theta)$ be a vector function of the parameter vector θ to estimate. Then, the CRB establishes that [28]

$$\mathbb{E}\left\{(z(\theta)-\hat{z}(\theta))(z(\theta)-\hat{z}(\theta))^{\mathrm{T}}\right\}\geq\mathbf{CRB}_z=\frac{\partial z(\theta)}{\partial\theta}^{\mathrm{T}}J^{-1}\frac{\partial z(\theta)}{\partial\theta},\tag{2}$$

where $\mathbf{CRB}_z$ is the matrix that represents the lower bound on the covariance of $z(\theta)$; J is the Fisher information matrix, which depends on the signal model; and the inequality means that the difference between the matrices is positive semi-definite. The unknown parameters are the elements of θ, and the inequality means that any unbiased estimator of a function of the DT elements (such as the FA, RA, its eigenvalues or eigenvectors) has an error variance not lower than the right term of Eq. (2).

It is shown in Appendix A that if we consider the signal model for the L-coil acquisition system developed in Section 2.2, the Fisher information matrix reduces to

$$J=C_L^2(p)G_\eta\Upsilon G_\eta^{\mathrm{T}},\tag{3}$$

where G_η is a matrix depending on the gradient field (direction and strength), the b value and the SNR, and Υ is a diagonal matrix depending on the sensitivity factor $C_L(p)$ and the SNR. Also, it can be shown that the Fisher information matrix reduces to the Rice case when a single-coil acquisition system is considered, as presented in Ref. [7].

Once J is computed, it is straightforward to obtain $\mathbf{CRB}_z$. Changing the function $z(\theta)$, we can obtain error bounds for some functions of the DT, such as the RA, the FA, the EAR, the eigenvalues and the eigenvectors, as shown below. It must be noted that J is a function of the gradient field scheme properties (strength and direction), the DT elements and the coil montage. Then, the CRB can be used to compare the performance bounds for different DT shapes, i.e., different relations among eigenvalues. Under certain regularity conditions, widely used algorithms such as maximum likelihood asymptotically achieve the CRB. Therefore, minimizing the CRB promises obtaining better performance from many estimation algorithms [28] through designing optimal measurement conditions.

2.2.1. Minimum mean square error

Let $\mathbf{D}$ be the DT under analysis. Since $\mathbf{D}$ is a 3×3 matrix, it is necessary to develop an appropriate metric that allows to quantify the distance between any estimator $\hat{D}$ and its true value $\mathbf{D}$. Then, the mean square error (MSE) under the Frobenius norm seems to be an appropriate choice [29]. The MSE is defined as

$$\mathrm{MSE}\left(\hat{D}\right)=\mathbb{E}\left\{||\hat{D}-D||_F^2\right\}.$$

In order to obtain the minimum MSE achievable by any estimator of the DT, it may be noted that

$$\begin{aligned}\mathrm{MSE}\left(\hat{D}\right)&=\mathbb{E}\left\{||\hat{D}-D||_F^2\right\}=\sum_{i,j=1}^{3}\mathbb{E}\left\{\left(D_{ij}-\widehat{D_{ij}}\right)^2\right\}\\&=\sum_{i,j=1}^{3}\mathrm{Var}\left\{\widehat{D_{ij}}\right\}\geq\sum_{i,j=1}^{3}\mathrm{CRB}\left(D_{ij}\right)\\&=\sum_{k=1}^{6}\xi_k\mathrm{CRB}_{kk}\triangleq\mathrm{MSE}_{min}\left(\hat{D}\right)\end{aligned}\tag{4}$$

where $\mathrm{MSE}_{\min}\left(\hat{D}\right)$ is the minimum MSE achievable by any unbiased estimator of $\mathbf{D}$, and ξ_k is 1 if $k=1,2,3$ or 2 if $k=4,5,6$. Then, using Eqs. (4) and (3), we can obtain the minimum error in the DT estimation, as well as its variation with the system parameters (i.e., gradient field setup and coil montage) and tensor shape (i.e., prolate, oblate or spherical).

2.2.2. Minimum standard deviation achievable in scalar parameters estimation

As mentioned in Section 1, the DT classification by means of scalar factors is of great interest in both theoretical analysis and

clinical applications. These factors can be the widely accepted RA, FA and EAR, defined as [18]

$$\mathrm{RA} = \sqrt{\frac{(\lambda_1-\lambda_2)^2+(\lambda_1-\lambda_3)^2+(\lambda_2-\lambda_3)^2}{(\lambda_1+\lambda_2+\lambda_3)^2}},$$

$$\mathrm{FA} = \sqrt{\frac{(\lambda_1-\lambda_2)^2+(\lambda_1-\lambda_3)^2+(\lambda_2-\lambda_3)^2}{2(\lambda_1^2+\lambda_2^2+\lambda_3^2)}},$$

$$\mathrm{EAR} = 1-\sqrt[p]{\frac{\lambda_1^p\lambda_2^p+\lambda_1^p\lambda_3^p+\lambda_2^p\lambda_3^p}{3\lambda_1^{2p}}}$$

where $\lambda_1 \geq \lambda_2 \geq \lambda_3$ are the eigenvalues of $\mathbf{D}$ and $p = 1.6075$.

If we replace $z(\theta)$ with the FA, RA or EAR definitions in Eq. (2), we can obtain the minimum standard deviation achievable by any unbiased estimator of these factors. Then, we can test the influence of the system acquisition setup and the DT shape in the lower bounds of these factor estimators. The bounds are used as a theoretical benchmark to choose among factors.

According to Eq. (2), it is necessary to evaluate the derivatives of these functions with respect to θ, which is easily done considering the reported results in Ref. [30].

2.2.3. Minimum standard deviation in the major eigenvector estimation

As mentioned before, analysis of errors in the estimation of the major eigenvector is of great importance in some DT-based studies, such as fiber tract reconstruction (see Ref. [3] and references therein). These errors are seen as angular variations in the estimated eigenvector, which usually determines the tract direction. Therefore, the computation of the CRB on the estimated eigenvector gives us very valuable information about the confidence region of the reconstructed tracts, taking into account the noise distribution.

Let q be the major eigenvector of $\mathbf{D}$, i.e., the eigenvector corresponding to λ_1. In Ref. [30], it is shown that $\mathbf{q} = \mathbf{a}/\|\mathbf{a}\|$, where

$$a = [(\theta_4\theta_6 - B\theta_5)(\theta_5\theta_6 - C\theta_4), (\theta_5\theta_6 - C\theta_4)(\theta_5\theta_4 - A\theta_6), (\theta_4\theta_6 - B\theta_5)(\theta_5\theta_4 - A\theta_6)]^T,$$

$A = \theta_1 - \lambda_1$, $B = \theta_2 - \lambda_1$, and $C = \theta_3 - \lambda_1$. Then, the CRB in the estimation of the major eigenvector ($\mathbf{CRB}_q$) is computed by considering $z(\theta) = q$ in Eq. (2).

Let $\hat{q}$ be an unbiased estimator of $\mathbf{q}$. Then, it can be shown [19,31] that the covariance matrix of this estimator is

$$\Sigma_{\mathbf{q}} = \omega_1 c_1 c_1^{\mathrm{T}} + \omega_2 c_2 c_2^{\mathrm{T}} + 0 q q^{\mathrm{T}},$$

where $\mathbf{c}_1$ and $\mathbf{c}_2$ are the eigenvectors of $\sum_q$ corresponding to the eigenvalues ω_1 and ω_2, respectively. This means that $\sum_q$ has rank 2, so $\hat{q}$ will only vary in the plane normally oriented to $\mathbf{q}$. If we assume $\hat{q} \sim N(\mathrm{q}, \sum_q)$, we can compute the ellipsoid that contains the estimates with probability P. This means that we can compute a confidence bound that ensures that the estimated eigenvector is contained inside it with a certain probability. It is known that the probability that the estimates of $\mathbf{q}$ are contained in the ellipsoid $x^{\mathrm{T}}{\Sigma_{\mathbf{q}}}^{-1}x = c^2$ is [32]

$$P = 1 - \frac{K}{\Gamma(\frac{K}{2}+1)2^{K/2}}\int_c^\infty x^K \exp\left(-x^2/2\right)\mathrm{d}x,$$

where K is the dimension of the ellipsoid (3 in the present analysis) and $\Gamma(\cdot)$ is the Gamma function. The mentioned ellipsoid encloses the ellipsoid $x^{\mathrm{T}}{\mathbf{CRB}_q}^{-1}x = c^2$, which is a theoretical bound, regardless of the used algorithm [32]. The latter is defined by the matrix $c^2\mathbf{CRB}_q$ and has semi-axes related to the eigenvector directions, with length equal to the square root of their corresponding eigenvalues. Since the eigenvalue of $\mathbf{CRB}_q$ corresponding to $\mathbf{q}$ is 0, the locus that denotes the theoretical bound is the ellipse with semi-axis $c\sqrt{\omega_1^{CR}}$ and $c\sqrt{\omega_2^{CR}}$, where ω_1^{CR} and ω_2^{CR} are the remaining eigenvalues of $\mathbf{CRB}_q$. This locus is usually depicted as the cone of uncertainty of the major eigenvector [19]. This is a valuable tool since it denotes local directional information and global structural information and is crucial in understanding changes in tissue microstructure as well as in white matter tracts [19]. Under the previous analysis, this cone represents the smallest region where the major eigenvector can be found with probability P.

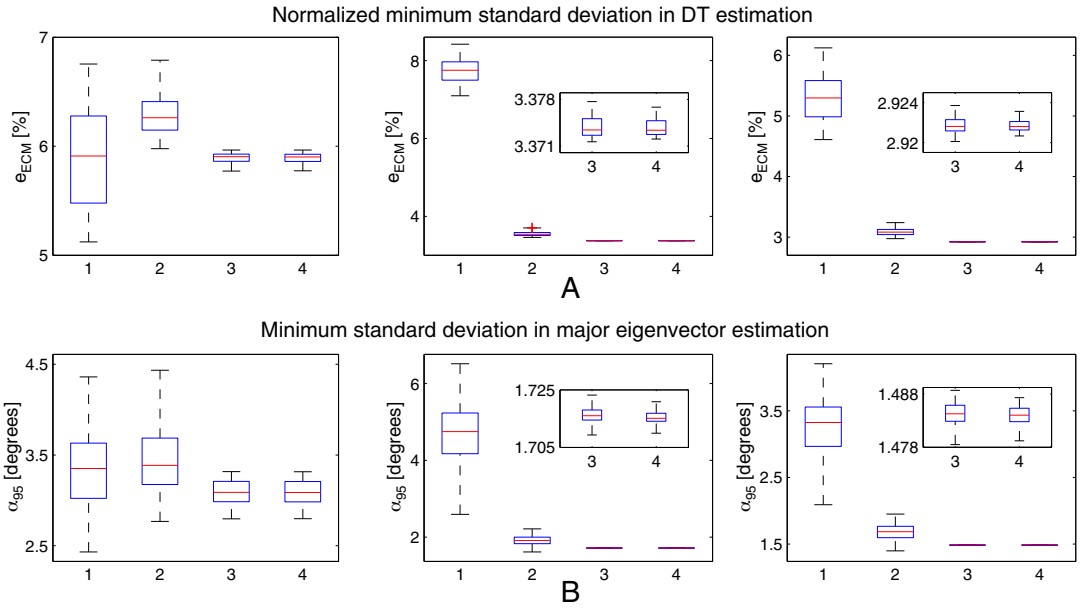

Fig. 1. Comparison between gradient field setups. We show the boxplot with the e_{MSE} (A) and the α_{95} (B) considering $N = 10$ (left), $N = 30$ (center) and $N = 40$ (right) gradient field directions, for a fiber-type DT ($\lambda_1 = 1 \times 10^{-3}$ mm^2/s and $\lambda_2 = \lambda_3 = 0.1 \times 10^{-3}$ mm^2/s) and a single-coil acquisition system. Each figure shows the results considering the setups proposed in 1 [5], 2 [16], 3 [17] and 4: [15]. We considered the typical values $b = 1200$ s/mm^2 and SNR = 30.

It is useful to compute the aperture angle of the cone, given by $\alpha_P = \text{atan}\left(cmax_j\sqrt{\omega_j^{CR}}\right)$. Then, if we consider $P = .95$, the theoretical minimum deviation in the estimation of the major eigenvector is bellow α_{95} with 95% probability.

3. Results

In this section, we use the presented framework to test the influence of measurement noise in DT estimation and in the functions of it. First, we show results considering synthetic data to test the DT estimation procedure and its variation with the gradient setup, the number of acquisition coils, the tensor shape, the SNR and the *b* value. Then we show these effects considering true DT-MRI data and obtain some conditions for an accurate estimation. Whenever assumed constant, we considered the typical values $b = 1200$ s/mm^2 and SNR $= 30$. We also assumed that the sensitivity pattern of each coil was homogeneous across the volume of interest [23].

In order to show results, we considered the coefficient of variation as a relative error measure. If A is a scalar function of the DT and σ_A^{MIN} is the minimum standard deviation in the estimation of A (given by its CRB), then the coefficient of variation relative to A is given by $e_A = \frac{\sigma_A^{\min}}{A} \times 100$. We also defined $e_{MSE} = MSE_{\min}^{1/2}\left(\hat{D}\right)/||D||_F \times 100$ to be consistent.

3.1. Results using synthetic data

To evaluate the developed performance bounds, we simulate synthetic DT data with different shapes and in approximately 1000 directions uniformly distributed along one spherical hemisphere. According to Eq. (3), the CRB can be used to test the influence of noise in the DT estimation when the tensor shape, gradient scheme and other acquisition factors (such as the SNR and the *b* value) are changed. This is of special interest when comparing different acquisition setups, providing useful results that could lead to optimal experiment designing criteria.

3.1.1. Gradient field setup evaluation

The choice of a gradient field setup has different effects on the quality of tensor-derived quantities [15]. Then, the CRB can be used as a method to compare different gradient setups, allowing to evaluate the minimum variance achievable by an unbiased estimator of the DT and the functions of it. Several gradient setups have been proposed in the literature, many of them optimal in some sense. In Ref. [16], the authors propose a gradient field setup that minimizes the condition number of the DT-MRI transformation matrix that relates the DT coefficients and the apparent diffusion; in Ref. [5], the authors propose a gradient setup based on equal solid angle

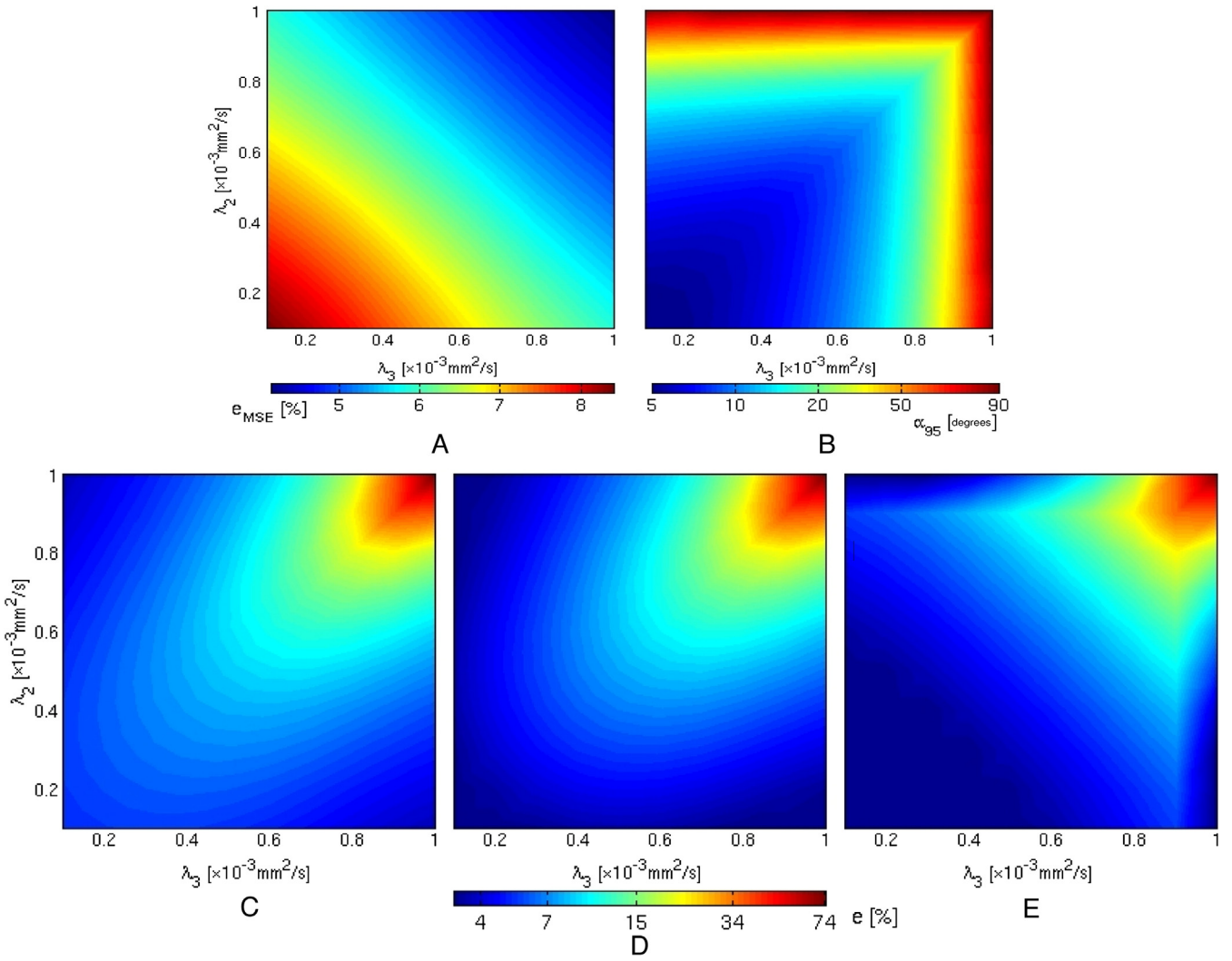

Fig. 2. Influence of tensor shape in DT estimation. We display the error bounds in the estimation of the DT scalar factors as a function of its two minor eigenvalues (λ_2 and λ_3 varying in $[0.1;1] \times 10^{-3}$ mm^2/s), keeping the major eigenvalue fixed to $\lambda_1 = 1 \times 10^{-3}$ mm^2/s, $N = 6$, and $L = 1$. We show the e_{MSE} (A), the α_{95} (B), the e_{RA} (C), the e_{FA} (D) and the e_{EAR} (E), as defined in Section 3. We considered the typical values $b = 1200$ s/mm^2 and SNR $= 30$.

weighting; in Ref. [17], the authors present a gradient field setup based on minimal electrostatic repulsive forces between point charges on a unit sphere; finally, in Ref. [15], the authors propose an efficient algorithm that allows to consider a gradient field setup uniformly distributed on a unit sphere.

In order to compare their performance, we computed the e_{MSE} and α_{95} scalar factors, which we used to evaluate the different gradient field setups. The e_{MSE} scalar factor allows to compare the minimum standard deviation in the estimation of the DT, while the α_{95} scalar factor allows to compare the angular errors associated with the major eigenvector estimation. In Fig. 1, we show a boxplot comparing e_{MSE} (Fig. 1A) and α_{95} (Fig. 1B), considering a different number of gradient directions (N), $N = 10$ (left), $N = 30$ (center) and $N = 40$ (right) for a fiber-type DT ($\lambda_1 = 1 \times 10^{-3}$ mm^2/s and $\lambda_2 = \lambda_3 = 0.1 \times 10^{-3}$ mm^2/s) and a single-coil acquisition system. Each figure shows the results for the setups presented in Refs. [5] (Setup 1), [16] (Setup 2), [17] (Setup 3) and [15] (Setup 4).

It can be seen that Setups 3 and 4 allow a better performance bound in the DT and major eigenvector estimation, obtaining smaller median (red lines inside boxes) and higher spatial uniformity (closer box limits) than the others. This is very important since the DT orientations may be unknown a priori, and the use of these setups may ensure uniformity of the errors regardless of its orientation. Although Setups 3 and 4 present similar performance bounds, we prefer to use Setup 4 because of its simplicity, computational cost and easy adaptability to the desired number of gradients. For this reason, we adopted Setup 4 for the rest of this work.

3.1.2. Influence of tensor shape

It is also of interest to evaluate the influence of the tensor shape in the estimation procedure. By tensor shape, we mean the ratios among eigenvalues. Since the DT is represented by an ellipsoid, we distinguish between prolate, oblate and spherical tensors, hereafter called fiber-type, disc-type and spherical-type tensors, respectively.

In Fig. 2, we show the error bounds in the estimation of the DT scalar factors as a function of the two smallest eigenvalues of the DT (λ_2 and λ_3 varying in $[0.1;1] \times 10^{-3}$ mm^2/s), keeping the largest eigenvalue fixed to $\lambda_1 = 1 \times 10^{-3}$ mm^2/s. Also, we considered six gradient directions and a single-coil acquisition system. We show the e_{MSE} (Fig. 2A), the α_{95} (Fig. 2B), the e_{RA} (Fig. 2C), the e_{FA} (Fig. 2D) and the e_{EAR} (Fig. 2E).

First, it can be seen from Fig. 2A that the normalized MSE is higher for fiber-type tensors (bottom-left corner), decreasing as their shape turn spherical (upper-right corner). However, the tensor shape drastically affects the major eigenvector estimates (Fig. 2B), growing as the tensor shape turns into a disk-type or a spherical-type, i.e., one or both smaller eigenvalues become closer to the major one.

Second, the direct comparison of the error bound in the estimates of the RA (Fig. 2C), the FA (Fig. 2D) and the EAR (Fig. 2E) allows us to elucidate the differences in order to select one of the anisotropy indices. It can be seen that the coefficient of variation corresponding to the FA is smaller than that corresponding to the RA, although their variations with the shape have a similar tendency. Nevertheless, it must be noted that the coefficient of variation corresponding to the EAR differs significantly from those corresponding to the RA and FA. It can be seen that the EAR has a lower bound for fiber-type tensors, while the FA (and even the RA) performs better for disc-type tensors. Therefore, the recommended scalar index may depend on the application and/or the brain region under analysis.

It must be mentioned that the relations shown in Fig. 2 hold when the number of gradient directions is increased, reducing their amplitude accordingly, as illustrated in Fig. 1. However, it is of great interest to test the influence of multiple-coil acquisition systems in the estimation of the DT and its related scalar factors, and their variations with the tensor shape. If we assume the noise in each coil to be independent and identically distributed (iid), the minimum standard deviation in the estimation (and, consequently, the coefficient of variation) considering l coils will decrease $\sqrt{l}$ times with respect to a single-coil system. However, the noise model stated in previous sections allows to consider the correlation among signals acquired with different coils. Then, it is of interest to evaluate the iid approximation and to study its significance in the proposed model. To do so, we define a single coefficient ρ to evaluate this in a simple way. Let $e_A(l)$ be the coefficient of variation of the parameter A considering l acquisition coils. Then we define

$$\rho_A = \left(\frac{\sum_{l=1}^{L} \left(e_A(1)/\sqrt{l} - e_A(l) \right)^2}{\sum_{l=1}^{L} e_A^2(l)} \right)^{1/2} \times 100,$$

where L is the total number of acquisition coils. Then, small ρ_A values will ensure the iid assumption when computing A.

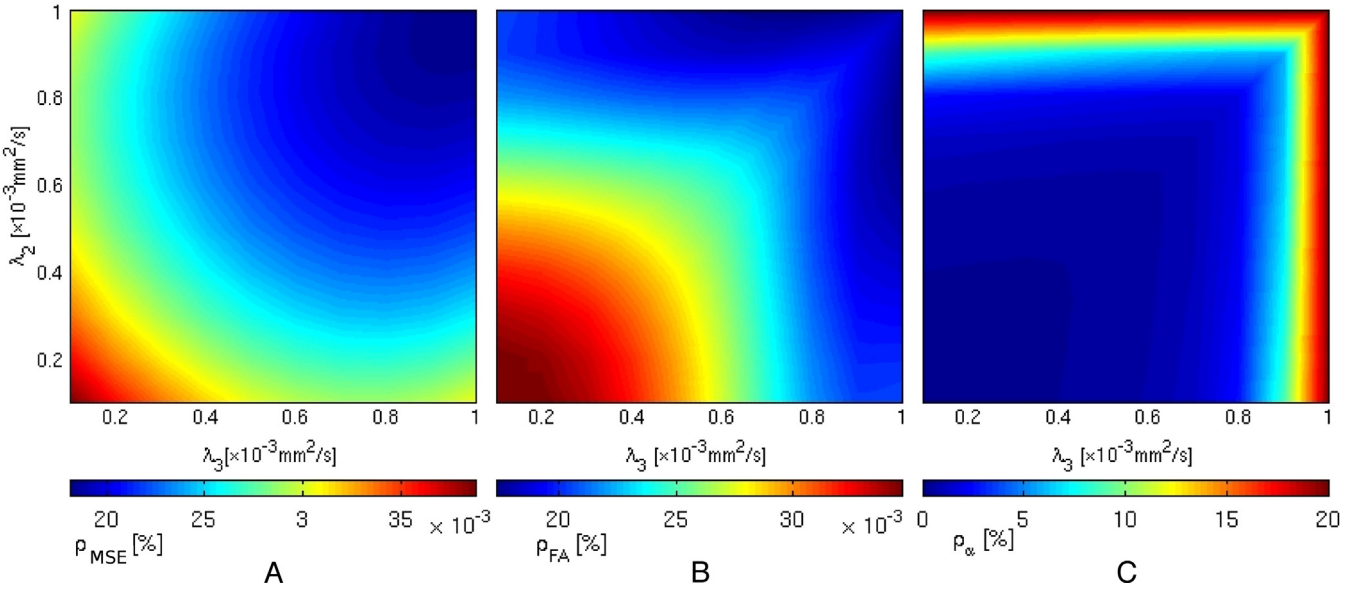

Fig. 3. Validation of the iid assumption. We show ρ_{MSE} (A), ρ_{FA} (B) and ρ_{α} (C) as a function of the minor eigenvalues, keeping the major fixed to $\lambda_1 = 1 \times 10^{-3}$ mm^2/s. We considered the typical values $b = 1200$ s/mm^2 and SNR = 30.

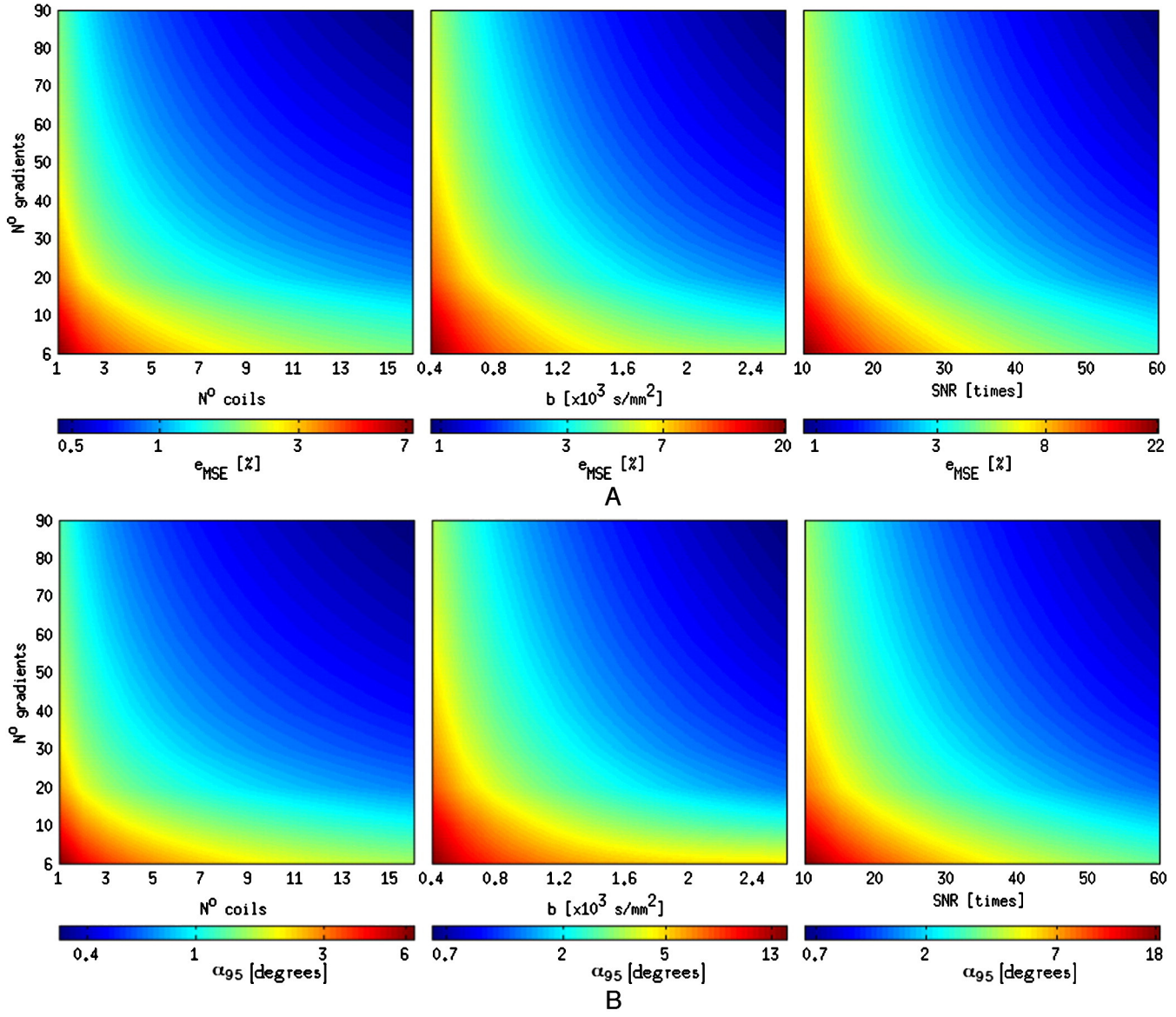

Fig. 4. Influence of the number of coils, the b value and the SNR in DT estimation. We show the e_{MSE} (A) and the α_{95} (B) as a function of the number of gradient directions and the number of coils (left), the b value (center) and the SNR (right). Black lines denote the contour lines, drawn only for comparison purposes. We considered $L = 1$, $b = 1200$ s/mm^2, and SNR $= 30$ whenever assumed constant. Whenever assumed constant, we considered the typical values $b = 1200$ s/mm^2 and SNR $= 30$.

The validity of the independent assumption as a function of the tensor shape is illustrated in Fig. 3. We show ρ_{MSE} (A), ρ_{FA} (B) and ρ_{α} (C) as a function of the minor eigenvalues, keeping the major fixed as in Fig. 2. It can be seen that the approximation is valid when considering the e_{MSE} (Fig. 3A) and the e_{FA} (Fig. 3B), where ρ takes values of approximately 0.03% (similar results are found for the e_{RA} and the e_{EAR}). However, this is not the case for α_{95} (Fig. 3C), where the iid assumption is valid for almost every tensor shape, but not all. Then, if we assume $\lambda_3 \leq \lambda_2 \leq 0.85\lambda_1$, the assumption can be accepted ($\rho_{\alpha}<5\%$). As a consequence, we can affirm that when estimating DT and the functions of it, we can reduce $\sqrt{l}$ times the performance bound when considering an l-coil acquisition montage, for almost every practical situation.

3.1.3. Influence of the SNR and the b value

Lastly, we proceed to evaluate the influence of the SNR and the b value. In Fig. 4, we show the e_{MSE} (Fig. 4A) and the α_{95} (Fig. 4B) as a function of the number of gradients and of the number of coils (left), the b value (center) and the SNR (right). We considered $L = 1$, $b = 1200$ s/mm^2 and SNR $= 30$ whenever assumed constant. Since Gaussian diffusion may be assumed only if $b < 3 \times 10^3$ s/mm^2 [33], we considered b values between 400 and 2500 s/mm^2. It can be seen that, although the SNR cannot be set by the user, their effects can be mitigated by increasing the number of acquisition coils and/or increasing the number of gradient directions and the b value. It must be mentioned that the influence of the SNR and the b value is practically constant when N changes, according to Fig. 1. Again, if we consider an l-coil acquisition system, this bound is reduced by $\sqrt{l}$ times.

3.2. Results using true data

We now proceed to evaluate the theoretical limits with real data. This allows to study the error bounds when performing the estimation in a real scenario situations. To do so, we use the IIT2 atlas[1] [34], which consists of an averaged DT map from 67 healthy

[1] Available at http://www.iit.edu/~mri/Home.html.

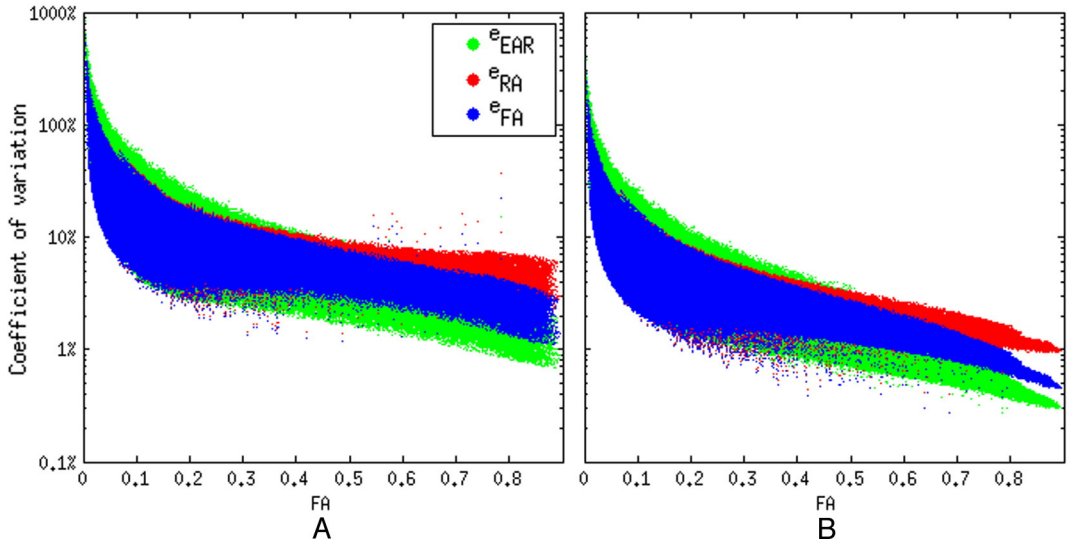

Fig. 5. Error in DT scalar functions estimation using true DT-MRI data. We show the e_{RA} (red), the e_{FA} (blue) and the e_{EAR} (green) factors as a function of the FA considering $N = 6$ (A) and $N = 30$ (B).

patients registered to the ICBM-152 atlas. First, we show the results over the whole volume of interest. Then, we perform an analysis that allows us to evaluate the spatial distribution of errors in the estimation procedure.

3.2.1. Results over the whole brain

We consider all the available data to evaluate the influence of the noise in the estimation of the DT and related parameters. In Fig. 5, we show the e_{RA}, the e_{FA} and the e_{EAR} computed in each voxel of the atlas for a single-coil acquisition system as a function of the FA considering $N = 6$ (Fig. 5A) and $N = 30$ (Fig. 5B). It can be seen that for tensors with FA >0.3, the minimum standard deviation in the EAR is lower than that corresponding to the FA and the RA. This is the case in almost every practical situation, since the general purpose in DT-MRI-based studies is to characterize the white matter, where the FA takes values greater than 0.3.

Next, we evaluate the minimum standard deviation in the major eigenvector estimation. As stated in Section 2, it depends on the spatial distribution of tensors and their shape. For this reason, we compute the empirical probability density function of α_{95} in the whole volume, $f_{\alpha 95}(\alpha_{95})$, which allows us to quantify the influence of measurement noise in the major eigenvector estimation as a function of the number of gradient directions and the number of coils. In Fig. 6, we show $f_{\alpha 95}(\alpha_{95})$ as a function of N assuming $L = 1$ (Fig. 6A) and as a function of L assuming $N = 30$ (Fig. 6B). We consider only tensors with FA >0.2, since these are the ones needed to perform tract-based studies. It can be seen that better major eigenvector estimation results can be achieved by incorporating more coils in the acquisition montage. For instance, the performance in the major eigenvector estimation can be doubled with respect to a single-coil considering an eight-coil system, as seen in the red curves. Moreover, increasing the number of acquisition coils should be preferable to increasing the number of gradient field directions.

Once $f_{\alpha 95}(\alpha_{95})$ is computed, we can get the limit of the 95% probability of α_{95}. This limit, defined as

$$\beta_{95} : \int_0^{\beta_{95}} f_{\alpha_{95}}(\alpha_{95}) d\alpha_{95} = 0.95,$$

asserts that 95% of the eigenvectors under study can be estimated with α_{95} lower than β_{95}. Since $f_{\alpha 95}(\alpha_{95})$ is a function of both L and N,

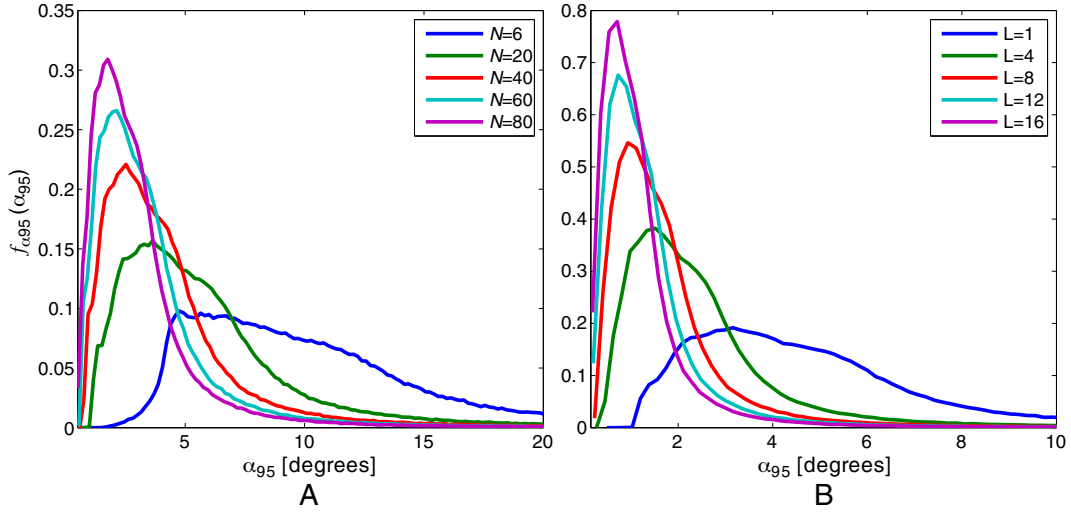

Fig. 6. Empirical probability density functions of α_{95}. We show $f_{\alpha 95}(\alpha_{95})$ as a function of α_{95} considering (A) $L = 1$ and different values of N, and (B) $N = 30$ and different values of L. Only tensors with FA >0.2 were considered.

β_{95} allows to evaluate the need of increasing these parameters according to the expected error. In Fig. 7, we show β_{95} as a function of the number of gradient directions and considering 1, 4, 8, 12 and 16 acquisition coils, depicted with different markers. It can be seen that the theoretical bounds decrease with both N and L, as expected. Also, Fig. 7 allows to determine the relation between both parameters in order to get a particular error. For example, since β_{95} is lower when considering $N = 10$ and $L = 8$ than when $N = 80$ and $L = 1$, it can be thought that it would be better (and faster!) to consider 10 gradient directions and an eight-coil acquisition system than a single-coil system and 80 gradient directions. Therefore, these results show the advantages of using a multiple-coil system in order to reduce the acquisition time without losing accuracy in the estimation.

3.2.2. Results in an axial slice

Finally, we show the results in an axial slice ($Z = 90$ in the MNI space). This allows to evaluate the advantages of the multiple-coil acquisition systems for DT estimation as a function of the voxel location in the brain and the number of gradient field directions considered. To do so, we considered only tensors with FA ≥ 0.1. In Fig. 8A, we show the e_{RA} (left), the e_{FA} (center) and the e_{EAR} (right) considering $N = 6$ (top) and $N = 40$ (bottom). The background image corresponds to the MRI-T2 provided with the atlas. It can be seen that the coefficients of variation are sensitive to the region under analysis since, as mentioned before, they depend of the tensor shape. To evaluate this situation, we show in Fig. 8B the coefficients C_l, C_e and C_d, defined as [35]

$$C_l = \frac{\lambda_1 - \lambda_2}{\lambda_1 + \lambda_2 + \lambda_3}, C_e = \frac{3\lambda_3}{\lambda_1 + \lambda_2 + \lambda_3}, C_d = \frac{2(\lambda_2 - \lambda_3)}{\lambda_1 + {}_2 + \lambda_3},$$

which allow to distinguish between fiber-type (high C_l), spherical-type (high C_e) and disc-type (high C_d) diffusion tensors. It can be seen that the coefficients of variation are high in regions where C_e is high, especially near the ventricles and in the interface between the gray and white matter. Also, it can be seen that the EAR is recommended in regions where the C_l is high, which are of special interest in white matter-related studies. As stated before, the use of an L coil acquisition system will reduce the coefficient of variation $\sqrt{L}$ times.

Finally, in Fig. 9, we show the e_{MSE} and the α_{95} considering $L = 1$ and $N = 6$, 20 and 50. It can be seen that the minimum standard deviation decreases notably when increasing the number of gradient field directions, especially in regions with high C_l. However, it may be noted that the angular error in the major eigenvector estimation cannot be reduced homogeneously as it happens with the MSE, since this error is higher than 32 degrees even when a 50-gradient field scheme is considered. Then, performing studies based on the eigenvectors should be done cautiously. The $\sqrt{L}$ times reduction is also valid in this region, although it may not be valid where C_e and C_d are high, where special care is needed.

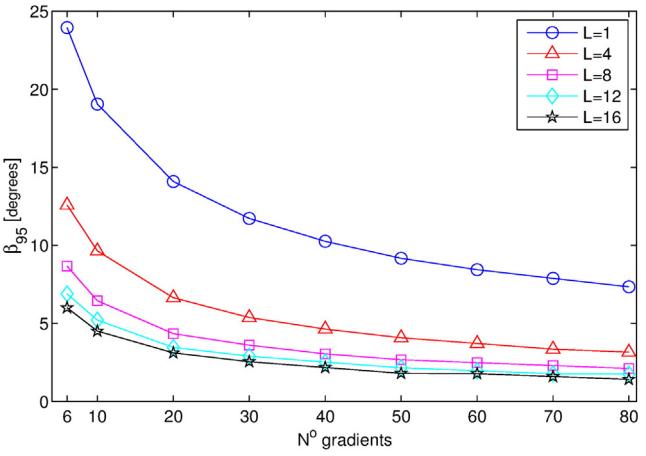

Fig. 7. Influence of multiple-coil systems in DT major eigenvector estimation. We present the β_{95} factor as a function of the number of gradient directions and considering 1, 4, 8, 12 and 16 acquisition coils, depicted with different markers.

4. Discussion

We presented a general framework to study the influence of noise in DT-MRI measurements when multiple-coil acquisition systems are used. Assuming the SoS signal model, we derive the performance bounds on the DT estimation and on the functions of it. This theoretical bound allows us to investigate the scope of DT-MRI-related studies, since it can be used as a tool that indicates the minimum variance achievable by any unbiased estimator of a function of the DT. Also, the CRB enables us to test the effect of many factors in the estimation performance, such as the number and direction of the applied gradient field, the number of acquisition coils, the tensor shape, the SNR and the b value.

The framework presented here differs from those frequently proposed in the literature, from the error propagation technique (see Refs. [5,6,36] among others) in the consideration of information regarding the noise distribution, and from the bootstrap method (see Refs. [37,38] among others) in its simplicity (there is no need for multiple acquisitions) and in obtaining parametric formulas that allow to make an accurate theoretical analysis. However, its greatest strength is that it permits performing an accurate analysis of the estimation procedure, independent of the estimation algorithm, and resulting in performance bounds valid for any unbiased method.

Based on the CRB, we first tested the influence of the gradient field setup used in DT-MRI acquisition. The setups proposed in Refs. [15] and [17] result in lower standard deviation bounds in the MSE and the α_{95}, i.e., in the whole DT and the major eigenvector estimation. They also provide higher spatial homogeneity and are therefore the preferred setups. This is in agreement with some existing works [39,40] where the gradient setup proposed in Ref. [17] is also recommended. In addition, the performance of the setup developed in Ref. [15] allows us to validate the hypothesis that the best results could be obtained by using gradients as uniformly distributed in the unit sphere as possible [41].

We presented results concerning the tensor shape and its effects in the DT estimates, as well as in scalar functions derived from it. We found that the minimal MSE attainable did not change drastically with the tensor shape, although the deviation in the estimates of the major eigenvector did. Also, we found that the minimum standard deviation associated with the FA was smaller than that corresponding to the RA, and its use is preferred, whenever possible. This is in accordance with some existing works [37,42] where only a few tensor shapes were studied. However, we showed that the EAR performs better than the FA and the RA when considering fiber-type tensors, which is of special interest when studying white matter abnormalities [43]. Again, this result agrees with previous reports [4,43]. The results presented here support the use of the EAR as a threshold factor in tractography studies.

The developed signal model allows us to study the influence of the number of acquisition coils in DT-MRI-derived studies. We found that the noise can be considered independent between coils when estimating all the DT-based functions, with the exception of the major eigenvector. However, this assumption became valid for tensors with C_l factor of medium to high, and then it can be assumed

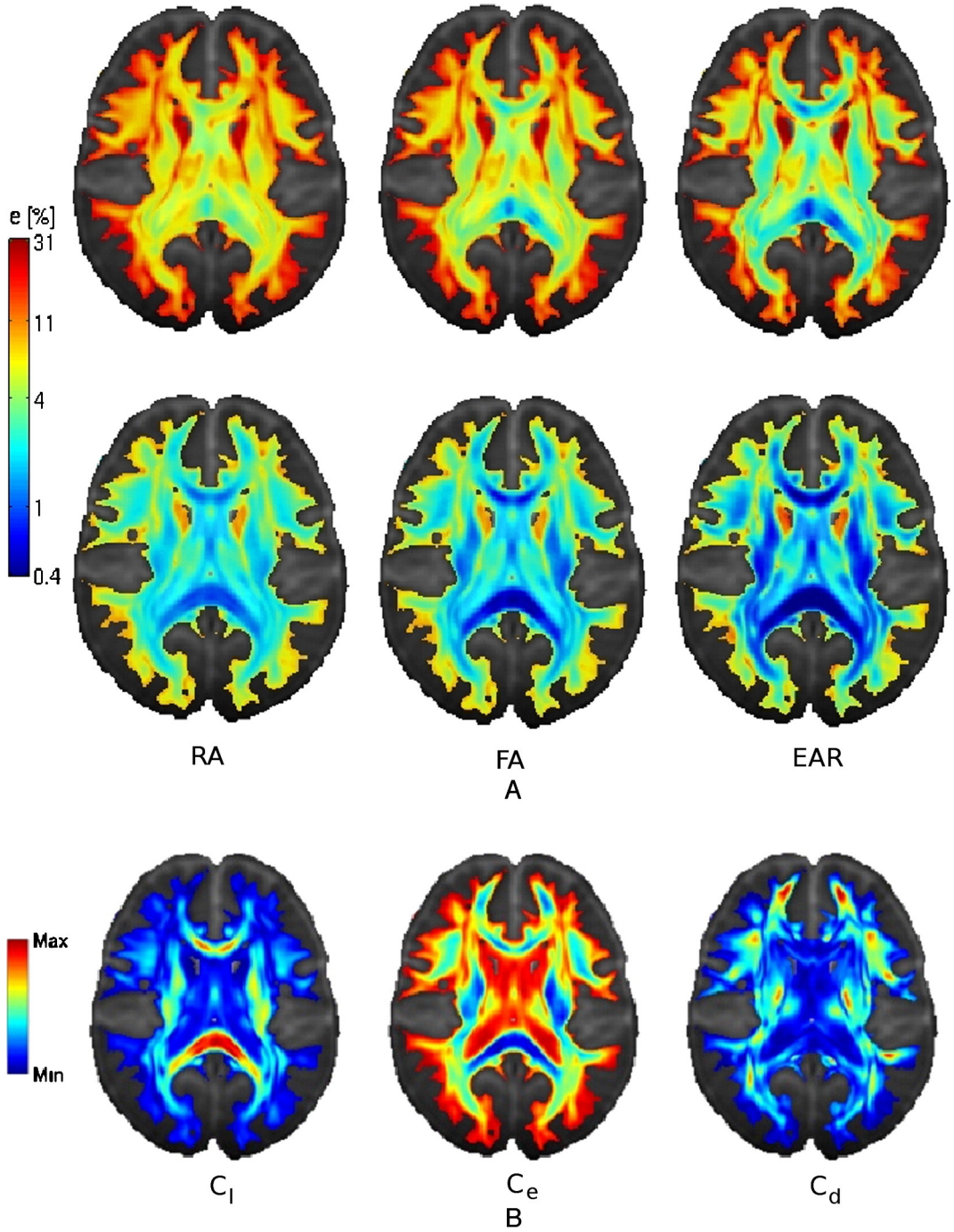

Fig. 8. (A) Errors in scalar indices estimation. We show the axial slices of e_{RA} (left), e_{FA} (center) and e_{EAR} (right) considering $N = 6$ (top) and $N = 40$ (bottom). The background image corresponds to the MRI-T2 provided with the IIT2 atlas. (B) Scalar indices C_l (left), C_e (center) and C_d (right), as defined in Section 3.2.

to be valid in almost all practical situations. Thus, we conclude that a reduction in the standard deviation by $\sqrt{L}$ times is attainable when using a system with an array of L coils.

We also studied the influence of uncertainties in the measurements in the major eigenvector estimation. This is very important since this vector is generally used in most deterministic tractography algorithms, such as in the streamlines tracking (STT) and fiber assignment by continuous tracking (FACT) techniques. We found valuable information regarding the system setup for reducing the angular error as much as possible. Results show that increasing the number of acquisition coils should be preferable to increasing the number of gradient field directions. This is relevant since it allows reducing the acquisition time spent in gradient field application by increasing the number of RF coils, without losing precision in the estimation procedure.

The CRB developed here has many other potential applications in DT-MRI-related studies. For instance, it can be used for designing purposes, since it is possible to find the optimum gradient direction scheme that minimizes the DT estimation variance for general and individual cases. This optimal design is useful to study the differences in optimal gradient schemes for different objectives, because it could happen that the best scheme for FA or EAR estimation differs from the best for eigenvector estimation. This study can be done using both the CRB and Wald tests, as usual in array signal processing-related studies [44].

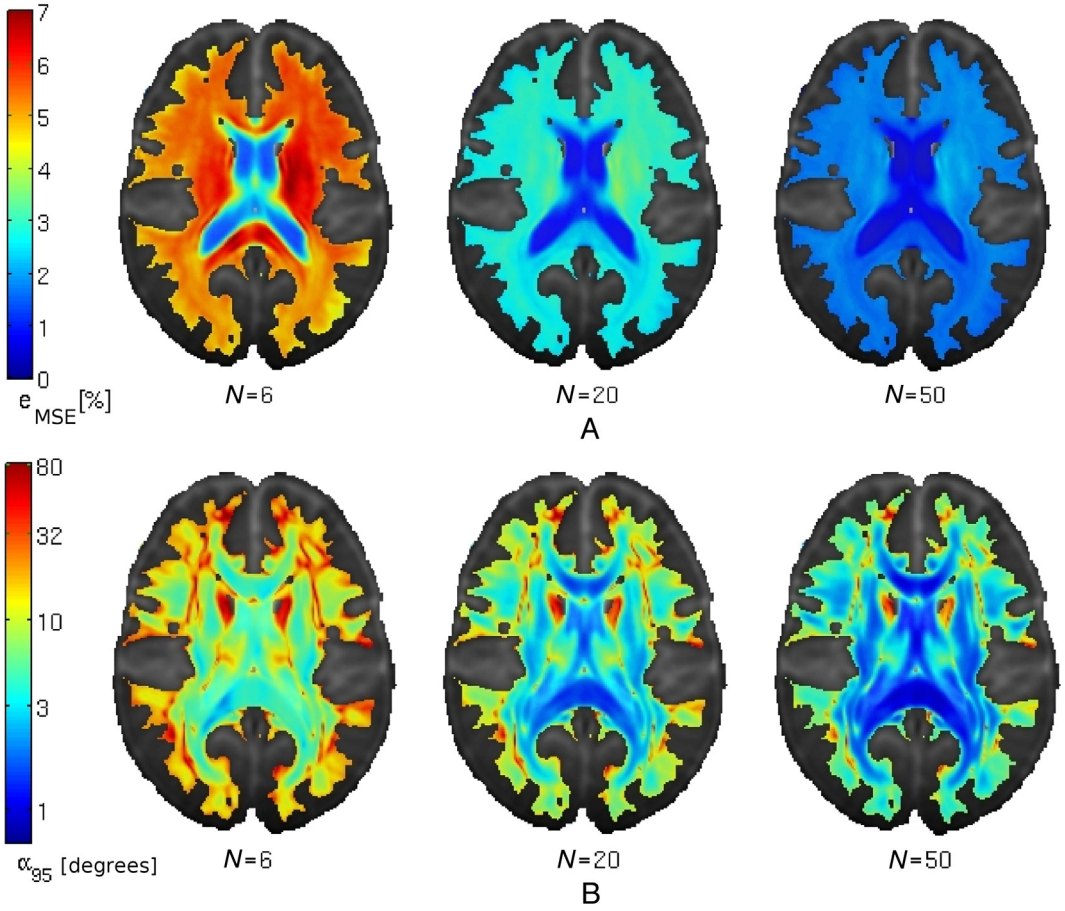

Fig. 9. Error in DT estimation as a function of the region of the brain under analysis. We show an axial slice of the e_{MSE} (A) and the α_{95} (B) factors considering $L = 1$ and $N = 6, 20$ and 50. The background image corresponds to the MRI-T2 provided with the IIT2 atlas.

The CRB can also be seen as a benchmark when comparing different DT estimation algorithms. Even though there exist plenty of DT estimation algorithms, there exists none that is uniformly best [45]. Therefore, the CRB serves a dual purpose: if an estimator is unbiased, the CRB tells how far it is from the best possible performance; if the estimator is biased, it could be used to test its improvement over the best unbiased estimator, justifying its choice. We plan to perform this analysis in future work.

Similarly, the framework presented permits to study performance bounds in the reconstruction of fiber tracts based on the DT model [3]. Unlike in Ref. [46] and in references therein, the proposed method makes it possible to study error bounds incorporating the noise distribution and regardless of the DT estimation algorithm. This can be done using the error variance in the major eigenvector for STT and FACT, or using the error variance in the whole DT when the tensor deflection algorithm (TEND) is used. We are currently performing this analysis. We also plan to study the validity of the constant $C_{\text{L}}(p)$ assumption by incorporating existing coil sensitivity patterns into our study. Generalizations to multitensor models (or other parametric models) will also be considered.

Appendix A

In this appendix, we show Eq. (3). The Fisher information matrix is defined as [28]

$$J_{ij} = -\mathbb{E}\left\{\frac{\partial^2 log(\mathcal{L})}{\partial\theta_i \partial\theta_j}\right\}, \tag{5}$$

where $\mathcal{L}$ is the likelihood function of the measurements and $\theta = [\theta_1 \ldots \theta_p]$ is the p-element vector to estimate. In the present case, we choose these parameters to be the elements of D, i.e., the six-element vector $\boldsymbol{\theta}$ defined in Section 2.1. In order to compute $\log(\mathcal{L})$, we assume N independent and identically distributed measurements, each one corresponding to a specific gradient direction. Then, using Eq. (1), it can be shown that the log-likelihood function is

$$\log(\mathcal{L}) = \sum_{n=1}^{N}\left(\log\left(\frac{A_{Tn}^{1-L}S_{Tn}^{L}}{\sigma^2}\right) + \log\left(I_{L-1}\left(\frac{A_{Tn}S_{Tn}}{\sigma^2}\right)\right) - \frac{S_{Tn}^2 A_{Tn}^2}{2\sigma^2}\right). \tag{6}$$

The CRB requires the *regularity condition* to hold, which determines that $\mathbb{E}\{\partial log(\mathcal{L})/\partial\theta_i\} = 0$. After some tedious but straightforward simplifications, it can be shown that this condition is equivalent to $\mathbb{E}\{S_{\text{T}n} I_L(\beta)/I_{L-1}(\beta)\} = A_{\text{T}n}$, where $\beta = A_{\text{T}n}S_{\text{T}n}/\sigma^2$. Then, it can be seen from Eq. (1) that this condition always holds.

The next step is to take the derivatives of Eq. (6) and compute its expected value. Again, after some algebra we get

$$J_{ij} = \sum_{n=1}^{N}\frac{1}{\sigma^4}\frac{\partial A_{\text{T}n}}{\partial\theta_i}\frac{\partial A_{\text{T}n}}{\partial\theta_j}\left(\mathbb{E}\left\{S_{\text{T}n}^2\frac{I_L^2(\beta)}{I_{L-1}^2(\beta)}\right\} - A_{\text{T}n}^2\right). \tag{7}$$

Let $\eta_{\text{n}} = A_{\text{n}}/\sigma$ be the SNR of the nth measurement and $\mathbf{G}_\eta$ the $6 \times N$ matrix defined as $\mathbf{G}_\eta = [\eta_1\mathbf{g}_1, \ldots\ \eta_N\mathbf{g}_N]$, where each $\mathbf{g}_{\text{n}}$ is a six-element vector given by

$$g_n = b\ \left[\gamma_{xn}^2, \gamma_{yn}^2, \gamma_{zn}^2, 2\gamma_{xn}\gamma_{yn}, 2\gamma_{xn}\gamma_{zn}, 2\gamma_{yn}\gamma_{zn}\right]^{\text{T}},$$

and $[\gamma_{xn}, \gamma_{yn}, \gamma_{zn}]^{\mathrm{T}}$ is the direction of the nth gradient field. Then, using Eq. (7) and previous definitions, we find the Fisher information matrix to be

$$J = C_L^2(p)\, G_\eta \Upsilon G_\eta^{\mathrm{T}},$$

where Υ is the diagonal matrix with $\{\Upsilon\}_{ii} = (C_L(p)\eta_i)^{1-L} Z(\eta_i, L, p) - C_L^2(p)\eta_i^2$ and

$$Z(\eta_i, L, p) = \int_0^\infty x^{2+L} exp\left(-\frac{x^2 + C_L^2(p)\eta_i^2}{2}\right) \frac{I_L^2(xC_L(p)\eta_i)}{I_{L-1}(xC_L(p)\eta_i)} \mathrm{d}x.$$

References

[1] Basser PJ, Mattiello J, LeBihan D. MR diffusion tensor spectroscopy and imaging. Biophys J 1994;66:259–67.
[2] Koay CG, Chang L-C, Carew JD, Pierpaoli C, Basser PJ. A unifying theoretical algorithmic framework for least squares methods of estimation in diffusion tensor imaging. J Magn Reson 2006;182:115–25.
[3] Mori S, van Zijl PCM. Fiber tracking: principles and strategies — a technical review. NMR Biomed 2002;15:468–80.
[4] Afzali M, Soltanian-Zadeh H. Comparison of voxel-based morphometry (VBM) and tractography of diffusion tensor MRI (DT-MRI) in temporal lobe epilepsy. 18th Iranian Conference on Electrical Engineering (ICEE), Iran; 2010. p. 18–23.
[5] Poonawalla A-H, Zhou X-J. Analytical error propagation in diffusion anisotropy calculations. J Magn Reson Imaging 2004;19:489–98.
[6] Koay CG, Chang L-C, Pierpaoli C, Basser PJ. Error propagation framework for diffusion tensor imaging via diffusion tensor representations. IEEE Trans Med Imaging 2007;26(8):1017–34.
[7] Alexander DC. A general framework for experiment design in diffusion MRI and its application in measuring direct tissue-microstructure features. Magn Reson Med 1997;60:439–48.
[8] Caan MWA, Khedoe HG, Poot DHJ, den Dekker AJ, Olabarriaga SD, Grimbergen KA, et al. Estimation of diffusion properties in crossing fiber bundles. IEEE Trans Med Imaging 2010;29(8):1504–15.
[9] Larkman DJ, Nunes RG. Parallel magnetic resonance imaging. Phys Med Biol 2007;52:R15–55.
[10] Gilbert G, Simard D, Beaudoin G. Impact of an improved combination of signals from array coils in diffusion tensor imaging. IEEE Trans Med Imaging 2007; 26(11):1428–36.
[11] Tristán-Vega A, Westin C-F, Aja-Fernández S. Bias of least squares approaches for diffusion tensor estimation from array coils in DT-MRI. Proc. 12th Intl. Conf. Med. Image Comp. Computer Assisted Interv., London, UK; 2009. p. 919–26.
[12] Aja-Fernández S, Trisán-Vega A, Casaseca de-la Higuera P. DWI acquisition schemes and diffusion tensor estimation: a simulation-based study. Conf. Proc. IEEE Eng. Med. Biol. Soc., Buenos Aires, Argentina; 2010. p. 3317–20.
[13] Giannelli M, Belmonte G, Toschi N, Pesaresi I, Ghedin P, Traino AC, et al. DT-MRI measurements of fractional anisotropy and mean diffusivity at 1.5 T: comparison of two radiofrequency head coils with different functional designs and sensitivities. Med Phys 2011;38(6):3205–11.
[14] Roemer PB, Edelstein WA, Hayes CE, Souza SP, Mueller OM. The NMR phased array. Magn Reson Med 1990;16:192–225.
[15] Koay CG, Hurley SA, Meyerand ME. Extremely efficient and deterministic approach to generating optimal ordering of diffusion MRI measurements. Med Phys 2011;38(8):4795–801.
[16] Skare S, Hedehus M, Moseley ME, Li T-Q. Condition number as a measure of noise performance of diffusion tensor data acquisition schemes with MRI. J Magn Reson 2000;147:340–52.
[17] Jones DK, Horsfield MA, Simmons A. Optimal strategies for measuring diffusion in anisotropic systems by magnetic resonance imaging. Magn Reson Med 1999; 42:515–25.
[18] Xu D, Cui J, Bansal R, Hao X, Liu J, Chen W, et al. The ellipsoidal area ratio: an alternative anisotropy index for DT-MRI. Magn Reson Imaging 2009;27:311–23.
[19] Koay CG, Nevo U, Chang L-C, Pierpaoli C, Basser PJ. The elliptical cone of uncertainty and its normalized measures in diffusion tensor imaging. IEEE Trans Med Imaging 2008;27(6):834–46.
[20] Jaermann T, Crelier G, Pruessmann KP, Golay X, Netsch T, van Muiswinkel AMC, et al. SENSE-DT-MRI at 3 T. Magn Reson Med 2004;51:230–6.
[21] Constantinides CD, Atalar E, McVeigh ER. Signal-to-noise measurements in magnitude images from NMR phased arrays. Magn Reson Med 1997;38(5): 852–7.
[22] Aja-Fernández S, Vegas-Sánchez-Ferrero G, Tristán-Vega A. About the background distribution in MR data: a local variance study. Magn Reson Imaging 2010;28:739–52.
[23] Dietrich O, Raya JG, Reeder SB, Ingrisch M, Reiser MF, Schoenberg SO. Influence of multi-channel combination, parallel imaging, and other reconstruction techniques on MRI noise characteristics. Magn Reson Imaging 2008;26(6):754–62.
[24] Griswold MA, Jakob PM, Heidemann RM, Nittka M, Jellus V, Wang J, et al. Generalized autocalibrating partially parallel acquisitions (GRAPPA). Magn Reson Med 2002;47:1202–10.
[25] Pruessmann KP, Weiger M, Scheidegger MB, Boesiger P. SENSE: Sensitivity encoding for fast MRI. Magn Reson Med 1999;44:952–62.
[26] Larsson EG, Erdogmus D, Yan R, Principe JC, Fitzsimmons JR. SNR-optimality of sum-of-squares reconstruction for phased-array magnetic resonance imaging. J Magn Reson 2003;163:121–3.
[27] Skare S. Optimisation strategies in diffusion tensor MR imaging. PhD thesis, MR Center, Dept. of Clinical Neuroscience, Karolinska Institutet, Sweden, 2002.
[28] Kay SM. Fundamentals of statistical signal processing: estimation theory. Signal processing series. New Jersey: Prentice-Hall; 1993.
[29] Smith ST. Covariance, subspace, and intrinsic Cramér-Rao bounds. IEEE Trans Sign Process 2005;53(5):1610–30.
[30] Hasan KM, Basser PJ, Parker DL, Alexander AL. Analytical computation of the eigenvalues and eigenvectors in DT-MRI. J Magn Reson 2001;152:41–7.
[31] Jeong H-K, Anderson AW. Characterizing fiber directional uncertainty in diffusion tensor MRI. Magn Reson Med 2008;60(6):1408–21.
[32] van Trees HL. Detection, estimation, and modulation theory. Part I. New York: John Wiley and Sons; 2001.
[33] Assaf Y, Basser PJ. Composite hindered and restricted model of diffusion (CHARMED) MR imaging of the human brain. NeuroImage 2005;27:48–58.
[34] Zhang S, Peng H, Dawe RJ, Arfanakis K. Enhanced ICBM diffusion tensor template of the human brain. NeuroImage 2011;54:974–84.
[35] Westin C-F, Peled S, Gudbjartsson H, Kikinis R, Jolesz FA. Geometrical diffusion measures for MRI from tensor basis analysis. ISMRM '97, Vancouver, Canada; 1997. p. 1742.
[36] Hasan KM. A framework for quality control and parameter optimization in diffusion tensor imaging: theoretical analysis and validation. Magn Reson Imaging 2007;25(8):1196–202.
[37] Hasan KM, Alexander AL, Narayana PA. Does fractional anisotropy have better noise immunity characteristics than relative anisotropy in diffusion tensor MR? An analytical approach. Magn Reson Med 2004;51:413–7.
[38] O'Gorman RL, Jones DK. Just how much data need to be collected for reliable bootstrap DT-MRI? Magn Reson Med 2006;56:884–90.
[39] Jones DK. The effect of gradient sampling schemes on measures derived from diffusion tensor MRI: a Monte Carlo study. Magn Reson Med 2004;51:807–15.
[40] Mang SC, Gembris D, Grodd W, Klose U. Comparison of gradient encoding directions for higher order tensor diffusion data. Magn Reson Med 2009;61(2): 335–43.
[41] Mukherjee P, Chung SW, Berman JI, Hess CP, Henry RG. Diffusion tensor MR imaging and fiber tractography: technical considerations. AJNR Am J Neuroradiol 2008;29(5):843–52.
[42] Papadakis NG, Xing D, Houston GC, Smith JM, Smith MI, James MF, et al. A study of rotationally invariant and symmetric indices of diffusion anisotropy. Magn Reson Imaging 1999;17(6):881–92.
[43] Kang X, Herron TJ, Woods DL. Validation of the anisotropy index ellipsoidal area ratio in diffusion tensor imaging. Magn Reson Imaging 2010;28:546–56.
[44] Dogandzic A, Nehorai A. EEG/MEG spatio-temporal dipole source estimation and array design. In: Hua Y, Gershman AB, Cheng Q, editors. High-resolution and robust signal processing. New York: Marcel Dekker; 2004. p. 393–442 Ch. 7.
[45] Landman BA, Mori S, Prince JL. Systematic evaluation of linear and nonlinear DTI estimation methods: an open framework. Intl Soc Magn Res Med, Berlin, Germany 2007.
[46] Lazar M, Alexander AL. An error analysis of white matter tractography methods: synthetic diffusion tensor field simulations. NeuroImage 2003;20:1140–53.